Journal of Marine Science and Technology
https://doi.org/10.1007/s00773-021-00837-7

ORIGINAL ARTICLE

Water quality modeling in subtropical shallow waters to predict environmental impacts of ocean thermal energy conversion

Ryota Oshimi[1] · **Shigeru Tabeta**[1] · **Katsunori Mizuno**[1]

Received: 29 January 2021 / Accepted: 2 July 2021

Abstract
Ocean thermal energy conversion (OTEC) is a power generation technology that extracts energy from the temperature difference between deep seawater and surface water in the ocean. Currently, a 100 kW class OTEC demonstration project is underway on Kume Island, Okinawa, and a plan to increase water intake and introduce a 1 MW class OTEC plant is under consideration. Year-round generation of electricity by an OTEC plant requires that it be installed in tropical and subtropical regions, where the surface water has a high temperature and low nutrient content. However, the water discharged from an OTEC plant will have the opposite characteristics of low water temperature and high nutrients, as well as a low pH. One of the most concerning environmental impacts of this discharged water is its influence on corals, which are important species in tropical and subtropical marine ecosystems. In this study, we developed an ecosystem model for a subtropical shallow-water region; the model combines a pelagic submodel, a chemical equilibrium submodel, and a benthic submodel, and successfully reproduces the observed variation in pH. The model was used to predict the environmental impact of water discharged from OTEC plant. The simulation results suggest that a 1 MW class OTEC plant would cause few environmental changes that would affect corals.

Keywords Coral · pH · Kume Island · Deep seawater

1 Introduction

Ocean thermal energy conversion (OTEC) is a power generation technology that extracts energy from the temperature difference between deep seawater and ocean surface waters. OTEC is currently viewed as a promising marine renewable energy source for tropical or subtropical regions, and the development of a 100 kW class OTEC demonstration project is now underway on Kume Island, Okinawa. Okinawa Prefectural Deepsea Water Research Center on Kume Island was opened in 2000, and research has been ongoing on the use of deep seawater, mainly in the fields of fisheries and agriculture. In 2012, the OTEC demonstration project was initiated, and it has achieved stable power generation since then. Deep seawater now plays an important role in supporting industry and employment in Kume Island, but the availability of deep seawater is currently insufficient to further revitalize the town. Therefore, a plan is under consideration to increase water intake and to introduce a 1 MW class OTEC plant. The technology for the utilization of deep seawater on Kume Island, including an OTEC plant, is an achievement of excellence in the international view [1].

Multiple-use technologies of deep seawater are characterized by their ability to provide a stable supply of electricity and drinking water, as well as to revitalize agricultural and fisheries industries. These features are considered compatible with small island developing states that face challenges such as high dependence on fossil fuels, food shortages, and the risk of potable water depletion [2]. The agencies on Kume Island are looking forward to exporting multiple-use technology of deep seawater to tropical and subtropical islands as green infrastructure. The trials on Kume Island are called the "Kumejima Model" and are approached from various perspectives, such as "a model for local production of food and energy," "a model for an environmentally friendly cycle-oriented society," and "a model as a self-sustaining island economy," in an attempt to demonstrate the superiority of this model, both domestically and internationally [3].

✉ Shigeru Tabeta
tabeta@k.u-tokyo.ac.jp

[1] The University of Tokyo, Kashiwa, Japan

Published online: 11 July 2021

Although OTEC has a promising future for tropical and subtropical islands, it raises concerns about the environmental impact of the water discharged from the OTEC plant. In general, surface waters in the tropics and subtropics have a high temperature and low nutrient content, whereas water discharged from an OTEC plant retains the characteristics of the deep seawater and is low in temperature and nutrient-rich. In addition, the surface water in tropical and subtropical regions has a pH of 7.9–8.2, while deep seawater has a pH of 7.3–7.6 [4]. Thus, the water discharged from an OTEC plant will have contrasting characteristics to the water quality in the surface water environment, raising concerns about adverse impacts on marine ecosystems. The influence on corals is one of the most concerning issues, as corals are an important species in tropical and subtropical marine ecosystems. In particular, corals have a calcium carbonate skeleton, and the calcification rate depends on the water pH [5–7].

The purpose of the present study was to develop an OTEC water quality model that considered pH. Despite concerns raised about changes in pH due to the discharge water from OTEC plants, previous studies on the discharge water from OTEC [8, 9] did not consider pH changes. Additional pH changes can also occur on a daily due to the photosynthesis of phytoplankton and the coral symbionts. Therefore, a water quality model was developed here to simulate pH changes due to the water discharged during OTEC, as well as the biochemical changes in the ecosystem. The model also considers the consumption of nutrients in the coral ecosystem, as nutrient variations also cause alkalinity changes.

2 Models

A coupled physical-ecosystem model was developed, in which the ecosystem model consists of a pelagic submodel, a benthic ecosystem submodel, and a chemical equilibrium submodel.

2.1 Physical processes

The MEC Ocean Model developed by the Marine Environment Research Committee of the Japan Society of Naval Architects and Ocean Engineers [10, 11] was used as the basis of the physical model. It is a three-dimensional hydrodynamic model with a z-coordinate system. The non-hydrostatic mode was used to simulate the density-driven flow of the water discharged from the OTEC plant.

2.2 Pelagic submodel

The pelagic submodel calculates the biochemical processes of the phytoplankton, zooplankton, detritus, and nutrients in the water environment. The phenomena considered by the model include phytoplankton photosynthesis and respiration, zooplankton predation and prey, and mineralization of organic matter. We implemented a modified NEMURO model [12], which includes total dissolved inorganic carbon and total alkalinity as compartments, as described by Yamanaka et al. (2004) [13].

The model consists of 15 compartments (Fig. 1). The phytoplankton PS and PL represent coccolithophores and diatoms, which have skeletons of calcium carbonate and silicon dioxide, respectively. ZS, ZL, and ZP represent zooplankton that have a certain prey relationship with PS and PL. NO_3, NH_4, $SiOH_4$, and Ca represent the nitrate, ammonia, silicate, and calcium ion nutrients present in the water. The detritus consists of particulate organic matter (PON) and dissolved organic matter (DON). The inorganic parts (such as the skeletons) of the plankton carcasses that originate from PS and PL are considered calcium carbonate ($CaCO_3$) and silicon dioxide (Opal), respectively.

Each compartment in the pelagic ecosystem model C_i follows the equation below.

$$\frac{\partial C_i}{\partial t} + u\frac{\partial C_i}{\partial x} + v\frac{\partial C_i}{\partial y} + w\frac{\partial C_i}{\partial z} = A_c\left(\frac{\partial^2 C_i}{\partial x^2} + \frac{\partial^2 C_i}{\partial y^2}\right) + \frac{\partial}{\partial z}\left(K_c\frac{\partial C_i}{\partial z}\right) + Q_i \quad (1)$$

(i = PS, PL, ZS, ZL, ZP, NO3, NH4, SiOH4, DON, PON, Opal, Ca, CaCO3, TCO2, TAlk).

Changes in the concentration C_i can be calculated by the physical processes (advection- diffusion) and biochemical processes Q_i, which are calculated as follows;

$$Q_{PS} = Gpp_{PS} - Res_{PS} - Mor_{PS} - Exc_{PS} - Gra_{PS\to ZS} - Gra_{PS\to ZL} \quad (2)$$

$$Q_{PL} = Gpp_{PL} - Res_{PL} - Mor_{PL} - Exc_{PL} - Gra_{PL\to ZL} - Gra_{PL\to ZP} \quad (3)$$

$$Q_{ZS} = Gra_{PS\to ZS} - Gra_{ZS\to ZL} - Gra_{ZS\to ZP} - Mor_{ZS} - Exc_{ZS} - Ege_{ZS} \quad (4)$$

$$Q_{ZL} = Gra_{PS\to ZL} + Gra_{PL\to ZL} + Gra_{ZS\to ZL} - Gra_{ZL\to ZP} - Mor_{ZL} - Exc_{ZL} - Ege_{ZL} \quad (5)$$

$$Q_{ZP} = Gra_{PL\to ZP} + Gra_{ZS\to ZP} + Gra_{ZL\to ZP} - Mor_{ZP} - Exc_{ZP} - Ege_{ZP} \quad (6)$$

$$Q_{NO3} = Nit - \left(Gpp_{PS} - Res_{PS}\right)\bullet R_{newS} - \left(Gpp_{PL} - Res_{PL}\right)\bullet R_{newL} \quad (7)$$

$$Q_{NH4} = -Nit - \left(Gpp_{PS} - Res_{PS}\right)\bullet\left(1 - R_{newS}\right) - \left(Gpp_{PL} - Res_{PL}\right)\bullet\left(1 - R_{newL}\right) + Exc_{ZS} + Exc_{ZL} + Exc_{ZP} + Rem_{DOM} + Rem_{POM} \quad (8)$$

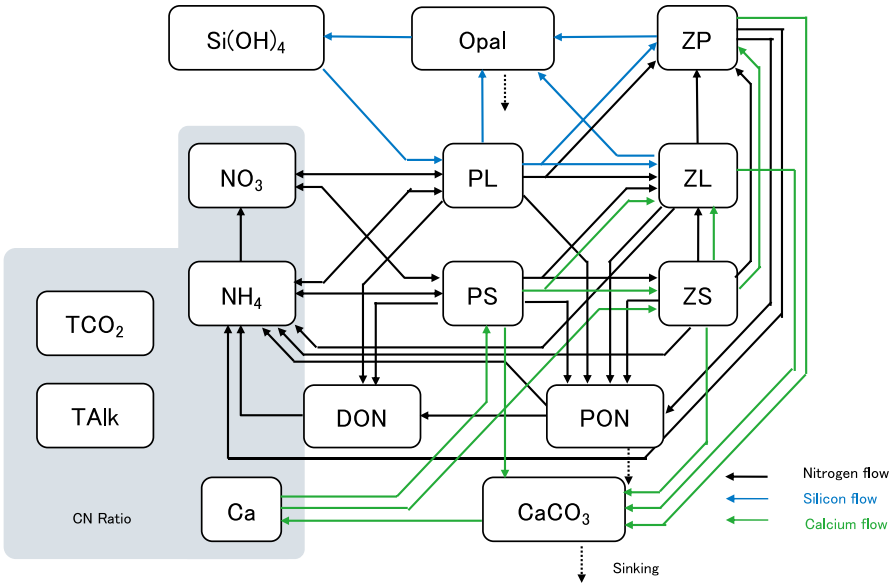

Fig. 1 Diagram of the pelagic submodel (modified from Yamanaka et al., 2004[13])

symbol	compartment	unit
PS	Small Phytoplankton	[μmol N/L]
PL	Large Phytoplankton	[μmol N/L]
ZS	Small Zooplankton	[μmol N/L]
ZL	Large Zooplankton	[μmol N/L]
ZP	Predatory Zooplankton	[μmol N/L]
NO_3	Nitrate	[μmol N/L]
NH_4	Ammonium	[μmol N/L]
$Si(OH)_4$	Silicate	[μmol Si/L]
PON	Particulate Organic Nitrogen	[μmol N/L]
DON	Dissolved Organic Nitrogen	[μmol N/L]
Opal	Particulate Opal	[μmol Si/L]
Ca	Calcium	[μmol Ca/L]
$CaCO_3$	Calcium Carbonate	[μmol Ca/L]
TCO_2	Total Dissolved Inorganic Carbon	[μmol C/L]
TAlk	Total Alkalinity	[μEq /L]

$$Q_{SiOH4} = -\left(Upt_{SiL} - Res_{PL} \bullet R_{SiN}\right) + Dec_{P\to Si}$$

$$+\left(Exc_{PL} + Gra_{PL\to ZL} + Gra_{PL\to ZP} + Mor_{PL}\right) \bullet R_{SiN} \quad (9)$$

$$Q_{PON} = Mor_{PS} + Mor_{PL} + Mor_{ZS} + Mor_{ZL} + Mor_{ZP} + Ege_{ZS} + Ege_{ZL}$$

$$+Ege_{ZP} - Dec_{P\to N} - Dec_{P\to D} - Sed_N \quad (10)$$

$$Q_{DON} = Exc_{PS} + Exc_{PL} + Dec_{P\to D} - Dec_{D\to N} \quad (11)$$

$$Q_{Opal} = (Mor_{PL} + Ege_{ZL} + Ege_{ZP} - Dec_{P2Si}) \bullet R_{SiN} - Sed_{Si} \quad (12)$$

$$Q_{Ca} = Dec_{CaCO3} - Frm_{PS} - Frm_{ZS} \quad (13)$$

$$Q_{CaCO3} = Mor_{PS} + Mor_{PL} + Ege_{ZS} + Ege_{ZL} + Ege_{ZP} - Dec_{CaCO3} \quad (14)$$

$$Q_{TCO_2} = \left(Q_{NO_3} + Q_{NH_4}\right)R_{CN} + Q_{Ca} \quad (15)$$

$$Q_{TAlk} = 2Q_{Ca} - Q_{NCO_3} + Q_{NH_4} \quad (16)$$

(*Gpp*: photosynthesis, *Res*: respiration, *Mor*: mortality, *Exc*: extracellular excretion, *Gra*: grazing, *Ege*: egestion, *Nit*: nitrification, *Rem*: remineralization, *Upt*: uptake, *Dec*: decomposition, *Sed*: sedimentation, *Frm*: Shell Formation. Units are mol L^{-1} s^{-1})

where R_{newS} and R_{newL} are the nitrogen consumption ratios for PS and PL, and R_{SiN} and R_{CN} are the Si:N and C:N ratios, respectively.

2.3 Chemical equilibrium submodel

A chemical equilibrium model for CO_2 system (CO2SYS) is used to calculate pCO_2 and pH from TCO2 and TAlk in the pelagic ecosystem model [14]. The model has four different scales for seawater pH (Total Scale, NBS Scale, free scale, and Sea Water Scale); however, most previous studies that have investigated pH effects on corals have used the Total Scale [15, 16]. Thus, in the present study, we used the Total Scale, which uses the concentration of $[H^+]$ considering all ions.

The partial pressure of carbon dioxide in the sea, pCO_2, is used to estimate the exchange rate of CO_2 between the atmosphere and the ocean. It is calculated by multiplying the fugacity of carbon dioxide by the fugacity factor K_0 [-]. The fugacity of carbon dioxide fCO_2 is calculated by the following formula

$$fCO_2 = \frac{\mathbf{pCO_2}}{K_0} \tag{17}$$

CO2SYS offers several choices for the parameters of the equation used to estimate the chemical equilibrium constants and salt concentrations. In this study, we used the parameters described by Dickson (1990) as the equilibrium constant for sulfuric acid, by Dickson & Millero (1987)[17] as the equilibrium constant for carbon dioxide, and by Uppstrom (1974)[18] for the total boron content.

2.4 Benthic submodel

The physical submodel, the pelagic ecosystem model, and the chemical equilibrium model described in the previous section can be used to simulate the temporal-spatial changes in pH. However, the high primary productivity of coral reefs results in strong effects on the actual seawater pH due to coral photosynthesis and calcification [19] calcification into the model. In addition, we considered a benthic ecosystem model that incorporated photosynthesis by macroalgae as well as coral photosynthesis and calcification [21].

Coral photosynthesis and calcification were calculated as changes in TCO2 and TAlk [22–24], as in the case of the pelagic ecosystem model.

The change in each compartment due to the benthic ecosystem processes is calculated in the layer just above the sea bottom, i.e., in the bottom layer. The value of Q_i in Eq. (1) is calculated as $Q_i + Q_{b,i}$. Here, $Q_{b,i}$ [mol L^{-1} s^{-1}] is the concentration change rate due to the benthic ecosystem processes, and i denotes NO_3, NH_4, Ca, TCO2, and TAlk. $Q_{b,\,i}$ is calculated based on the production rates of organic matter and of inorganic matter.

P_C and P_A [mol m^{-2} s^{-1}] are the photosynthetic rates of coral and macroalgae, respectively.

$$P_C = P_{maxC}\left(1 - e^{-I/I_{optC}}\right) - R_C \tag{18}$$

$$P_A = P_{maxA}\left(1 - e^{-I/I_{optA}}\right) - R_A \tag{19}$$

where P_{maxC}, P_{maxA} are the maximum photosynthesis rates of coral and algae, R_C, R_A are the respiration rates, and I is the light intensity in the bottom layer.

The production rate of inorganic matter G_C [mol m^{-2} s^{-1}] to generate the skeleton of calcium carbonate is:

$$G_C = G_{max}\left(1 - e^{-I/I_{optC}}\right) + G_{night} \tag{20}$$

where G_{night} is the calcification rate at night, and $G_{max} + G_{night}$ represents the calcification rate under sufficient light intensity. G_{max} and G_{night} can be written as follows using the calcium saturation state Ω_{Ar}:

$$G_{max} = k_{max}\left(\Omega_{Ar} - 1\right)^{n_{max}} \tag{21}$$

$$G_{night} = k_{night}\left(\Omega_{Ar} - 1\right)^{n_{night}} \tag{22}$$

$$\Omega_{Ar} = \frac{C^{2+} \bullet {CO_3}^{2-}}{K_{sp}} \tag{23}$$

The calcium ion concentration in seawater does not change much; therefore, calcium saturation is determined almost entirely by the carbonate ion concentration. The change rates of P_C, P_A, and G_C can be used to calculate the changes in Ca, NO_3, and NH_4.

Ca changes when an inorganic matter is generated, with a change rate $Q_{b,Ca}$ that can be written as follows.

$$Q_{b,Ca} = -G_C/\Delta z_b \tag{24}$$

where Δz_b is the thickness of the bottom layer.

The levels of NO_3 and NH_4 change when organic matter is produced. At first, the consumption of inorganic nitrogen is estimated from the consumption of organic carbon by photosynthesis. Next, the changes in NO_3 and NH_4 are calculated using the consumption ratio R_{new} for inorganic nitrogen:

$$Q_{b,NO_3} = -\frac{P_C/R_{CNc} + P_A/R_{CNa}}{\Delta z_b} \bullet R_{new} \tag{25}$$

$$Q_{b,NH_4} = -\frac{P_C/R_{CNc} + P_A/R_{CNa}}{\Delta z_b} \bullet \left(1 - R_{new}\right) \tag{26}$$

The CN ratio used to estimate nitrogen consumption from carbon consumption differs between benthic and

pelagic ecosystems. In the pelagic ecosystem model, the Redfield Ratio (C:N = 106: 16) is used as the CN ratio of phytoplankton. Conversely, the CN ratio of macroalgae, R_{CNa}, is set at 550:30 because the CN ratio differs for photosynthesis in seaweed beds [25]. Many uncertainties still remain for the nitrogen cycle of corals, and their high productivity, despite the poor levels of nutrients, has long been called Darwin's Paradox [26, 27]. The nutrients used by coral symbiotic organisms are reused inside the coral (nutrient recycling); therefore, estimates of the apparent CN ratio focus only on C and N taken in from outside the coral. This apparent CN ratio, R_{CNc}, was set at 8820:124, based on previous studies on CN circulation in coral [28, 29].

In this study, all N released from coral symbiosis is assumed to be taken up by the coral, whereas N released from coral is excreted as DON that forms membranes on the coral surface. DON is absorbed by sponges living in coral reefs and is released as PON from the sponges. This PON is consumed by filter feeders, such as crabs and shellfish, and then transferred to higher trophic levels. This pathway by which coral DON returns to the grazing cycle is called the sponge loop, and it plays a similar role to that of the microbial loop commonly found in oligotrophic open oceans [30–33]. Since the amount of nitrogen released directly from corals as inorganic nitrogen (NH_4 and NO_3) is very small compared to the amount of nitrogen released as DON and returning to the grazing cycle, all nitrogen released from the corals is assumed to enter the sponge loop.

The changes in TCO2 and TAlk, Q_{b,TCO_2} and $Q_{b,TAlk}$, in the benthic ecosystem are calculated in the same way in the pelagic model.

$$Q_{b,TCO_2} = \left(Q_{b,NO_3} + Q_{b,NH_4}\right)R_{CN} + Q_{b,Ca} \tag{27}$$

$$Q_{b,TAlk} = 2Q_{b,Ca} - Q_{b,NCO_3} + Q_{b,NH_4} \tag{28}$$

The parameters in the benthic model (Table 1) are determined according to Kleypas et al.[21], who described the photosynthetic rate and calcification rate of corals and macroalgae.

2.5 Other processes

The CO_2 dissolution from the atmosphere is also considered. The transfer rate F for CO_2 between the atmosphere and the sea is initially calculated using the following equation [34]:

$$F = \boldsymbol{\alpha} \bullet \kappa \bullet \left(pCO_{2sea} - pCO_{2air}\right) \tag{29}$$

where pCO_{2sea} and pCO_{2air} are the partial pressures of carbon dioxide in the sea and the atmosphere, respectively. The value of pCO_{2sea} is calculated at the surface grid in the pelagic model, and α[mol L^{-1} atm^{-1}] is the solubility of CO_2 in seawater, calculated as a function of the water temperature T [K] and salinity S [‰] [35], as follows:

$$\ln\boldsymbol{\alpha} = A_1 + A_2(100/T) + A_3\ln(T/100) + S\left[B_1 + B_2(T/100) + B_3(T/100)^2\right] \tag{30}$$

where κ [cm h^{-1}] is the gas transfer piston velocity, which can be written as a function of the wind speed u_{10} [m s^{-1}] at 10 m above sea level and the Schmidt number Sc, as follows [36]:

$$\kappa = 0.31 \bullet {u_{10}}^2 \bullet (Sc/660)^{-1/2} \tag{31}$$

A value of 0.31 is adopted for the coefficient in gas exchange rate [37]. The change in TCO2 at the surface grid is calculated by the following equation:

$$Q_{s,TCO_2} = F/\Delta z_s \tag{32}$$

where Δz_s is the thickness of the surface layer.

Table 1 Parameters in the benthic submodel

p_{maxC}	Coral maximum rate of production	0.0256	[μmol/m^2/s]
I_{optC}	Coral optimum light intensity of photosynthesis	54.7	[μmol/m^2/s]
r_C	Coral respiration rate in dark	0.0078	[μmol/m^2/s]
p_{maxA}	Macroalgal maximum rate of production	0.0222	[μmol/m^2/s]
I_{optA}	Macroalgal optimum light intensity of photosynthesis	109.4	[μmol/m^2/s]
r_A	Macroalgal respiration rate in dark	0.007	[μmol/m^2/s]
k_{max}	Coral coefficient of maximum calcification rate	0.0025	[μmol/m^2/s]
n_{max}	Coral reaction order of maximum calcification rate	1.0	[-]
I_{optCC}	Coral optimum light intensity of calcification	87.5	[μmol/m^2/s]
k_{night}	Coral coefficient of calcification rate in dark	0.0008	[μmol/m^2/s]
n_{night}	Coral reaction order of calcification rate in dark	1.0	[-]

2.6 Computational conditions

The computational domain was a coastal area of 2 km × 2.5 km in the northeastern part of Kume Island in Okinawa Prefecture (Fig. 2). The computational grid was created with reference to the water depth data by the Japan Hydrographic Association. The maximum depth was 250 m, with 21 vertical layers. The grid size in the horizontal direction was set at 25 m (80 × 100 grids). To avoid the non-physical reflection along the open sea boundary, a buffer zone with numerical dumping is applied. The target sea area has steep terrain, so dummy grids were added along the outside boundaries of the computational area to ensure computational stability. In the dummy grid, the viscosity coefficients were set to gradually increase in an outward direction.

For tides, the four major constituents (M2, S2, O1, and K1) were given, and their amplitudes were tuned to match the actual current velocity. The meteorological observation data for temperature, air pressure, solar radiation, cloudiness, relative humidity, precipitation, and wind velocity were obtained for June 28 to July 7, 2017 at the Kumejima observatory of the Japan Meteorological Agency and used to calculate the surface fluxes.

The initial and boundary conditions of the vertical profiles of the water temperature and salinity were obtained from the climatology listed in the World Ocean Atlas. Nutrient data were taken from an assessment report of OTEC in Kumejima. DIC and organic matter were estimated from the information of other subtropical regions [38, 39] because no observational data were available for the Kume Island region. The ranges of each variables used for the initial and boundary conditions are shown in Table 2.

The benthic ecosystem model requires data for the coral coverage. Based on the field observation, we assumed that the coral habitat is limited to a water depth from 0 to 40 m, with a coral coverage of 60% [40].

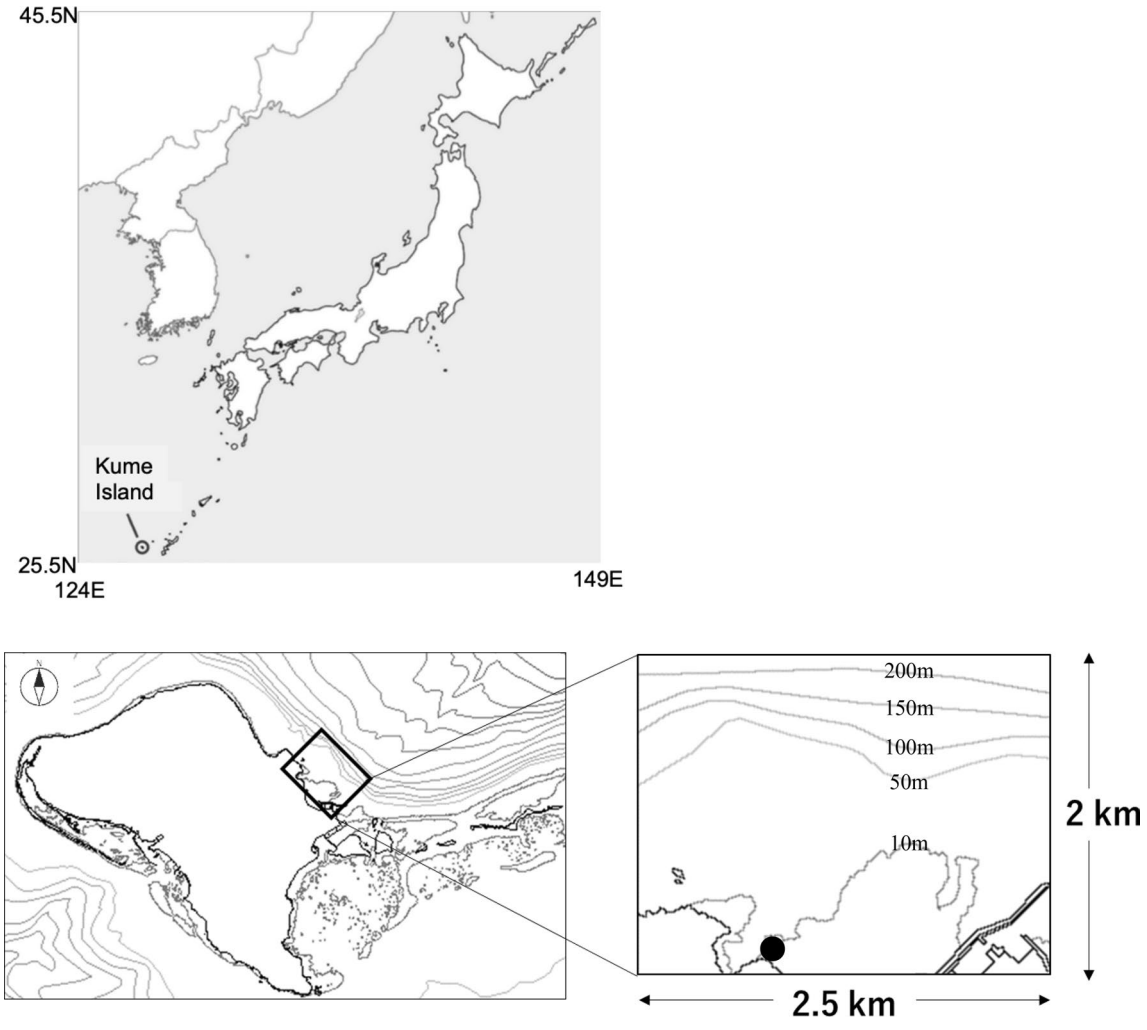

Fig. 2 The location of Kume Island (top), geometry of Kume Island (bottom-left) and the computational domain (bottom-right). The ● symbol in the bottom-right figure indicates the discharge point of OTEC plant

Table 2 The ranges of pelagic variables for the initial and boundary conditions

variables	Values (at the depth of 0–250 m)	variables	Values (at the depth of 0–250 m)
T	29.10—17.57 ℃	Si(OH)4	1.8–3.2 µmol Si/L
S	34.38–34.79	PON	0.11–0.038 µmol N/L
PS	0.11–0.0 µmol N/L	DON	5.5–4.0 µmol N/L
PL	0.011–0.0 µmol N/L	Opal	0.010–0.0095 µmol Si/L
ZS	0.0056–0.0 µmol N/L	Ca	0.010–0.010 mol Ca/L
ZL	0.0056–0.0 µmol N/L	CaCO3	8.2–0.50 µmol Ca/L
ZP	0.00056–0.0 µmol N/L	TCO2	1915—2102 µmol C/L
NO3	0.14–2.2 µmol N/L	TAlk	2250–2306µEq/L
NH4	0.050–0.055 µmol N/L		

3 Model behavior

3.1 Diurnal changes

Figure 3 shows a time series of pH and coral photosynthetic rate in a grid at a depth of 4 m in a coral-inhabited area at which the temporal changes are clearer. The pH rises as CO_2 is consumed by photosynthesis during the daytime, and it declines as CO_2 is released by respiration during the night time. The pH reaches its peak in the late afternoon. These results are consistent with previous observations of coral photosynthesis [19].

Figure 4 shows the diurnal changes in the horizontal distribution of pH and NO_3 on the grid just above the seafloor. The pH reaches a maximum in the late afternoon and a minimum around dawn in the entire shallow area shown in the time series. The concentration of NO_3 decreases when CO_2 is consumed. The difference in horizontal distribution of NO_3 with and without the coral model at late afternoon is shown in Fig. 5. The concentration of NO_3 with coral model became lower than that without coral model. These results indicate that the modeling of the nitrogen consumption process by corals is also functioning properly.

3.2 Comparison of simulations and experimental observations

The results of the simulation were compared with previously published observations [19]. We could not find any good information for the direct comparison, e.g. pH observation with other information necessary for the simulation. Thus the ranges of diurnal variation is discussed here. The change in pH calculated by the pelagic submodel corresponded closely to the change due to phytoplankton-related phenomena; therefore, the results by the pelagic submodel (Fig. 6a) was compared with the observed value in the open ocean in subtropical regions (Fig. 6b). The change in pH calculated by the benthic submodel (Fig. 6c) closely corresponded to the change due to coral, so it was compared with the observation in coral reefs (Fig. 6d).

Both comparisons showed that the simulation results were consistent with the observations. The pelagic model showed a quite small variation in pH, similar to the variations in the observations made for the open ocean. The range of pH values calculated by the benthic model was close to the values observed in coral reefs. To get the necessary data for the simulation at the specific location and conduct direct comparison will be the future task.

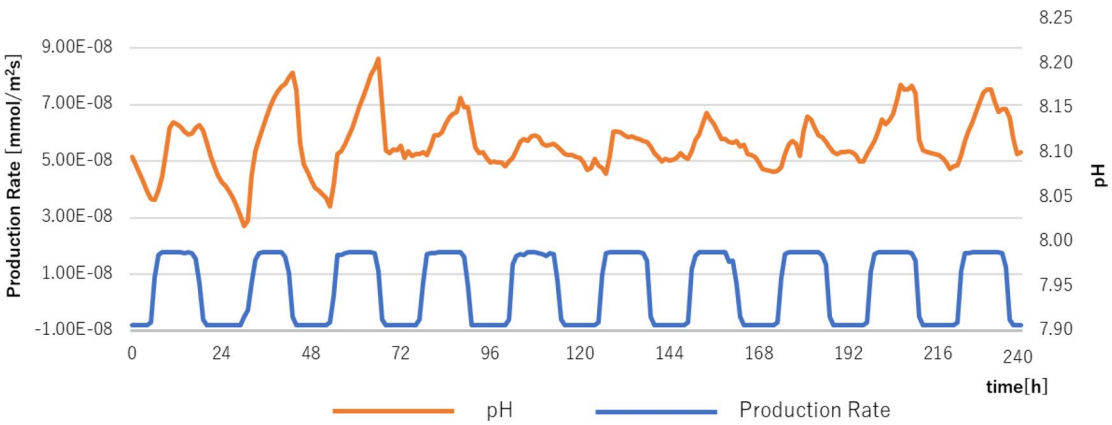

Fig. 3 Time series of pH in a coral-inhabited area and coral photosynthetic rate

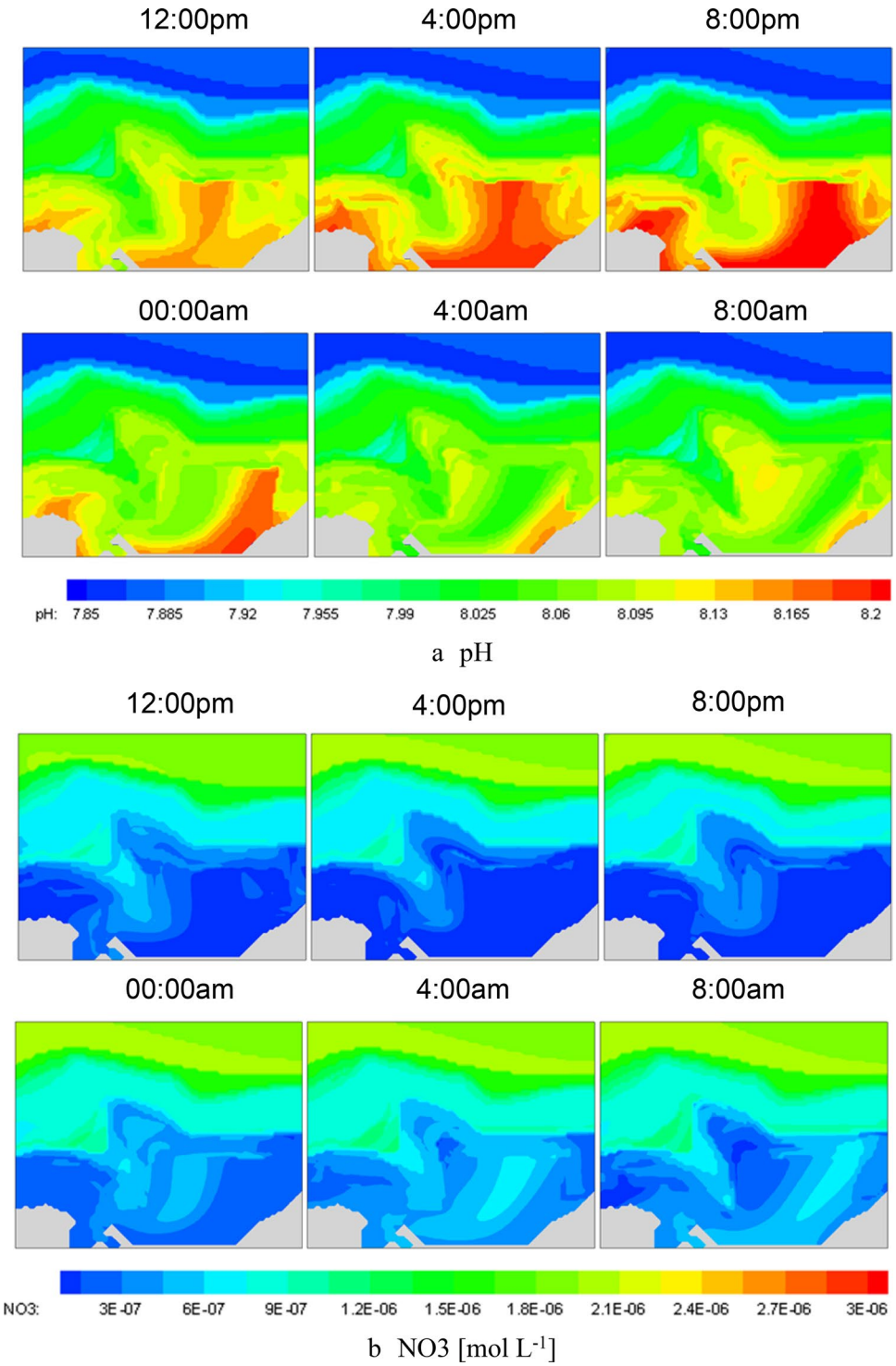

Fig. 4 Diurnal changes in horizontal distributions of pH and NO_3 in seawater from the grid just above the seafloor

3.3 Contribution of each biological process to pH

The changes in pH are caused by biological processes such as photosynthesis, calcification, respiration, and so on. In the model, a change in pH is derived from changes in TCO2 and TAlk. We investigated how each biological process in the pelagic and benthic model contributes to TCO2 and TAlk.

The Q_{TCO2} calculated in the pelagic model changes during the day, as shown in Fig. 7a. Looking at the breakdown (Fig. 7c), TCO2 increased (Q_{TCO2} becomes positive) throughout the day at an almost constant rate due to the effects of respiration and mineralization of organic matter. In the pelagic model, the dissolution of $CaCO_3$ was more prominent than its generation, resulting in increased TCO2 in

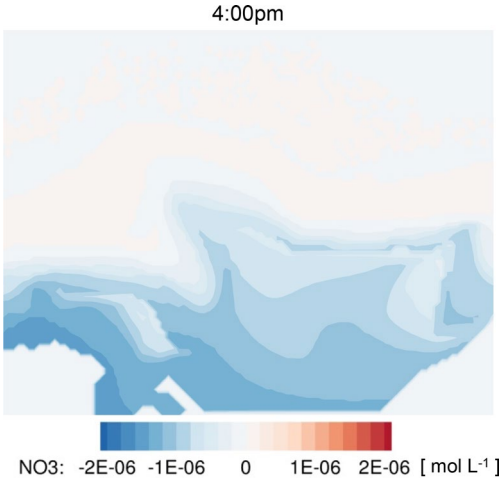

Fig. 5 Difference in horizontal distribution of NO_3 in the grid just above the seafloor with and without the coral model

the seawater. TCO2 was also consumed during the daytime because of photosynthesis. The rate of change in TCO2 was confirmed to account for a larger proportion of the change in organic matter due to photosynthesis and respiration than due to the generation and dissolution of $CaCO_3$.

The variable range of pH calculated by the pelagic and benthic models differed in scale, but both models showed similar patterns of diurnal variation. However, the rates of change in TAlk and TCO2 by the pelagic and benthic models were different. Figures 7c and 8c show that the changes in Q_{TCO2} related to $CaCO_3$ are opposite for the pelagic and benthic submodels. These values are more likely to be determined by changes in the inorganic matter than in organic matter. The sign of Q_{TAlk} is always reversed in Figs. 7b and 8b. This is because the benthic model considers only the generation of $CaCO_3$, whereas the pelagic model deals with both the generation and decomposition of $CaCO_3$. Whether this is the case in actual waters is not known, but it could be a realistic assumption because suspended $CaCO_3$ reportedly has a higher dissolution rate than sedimented $CaCO_3$ [41, 42].

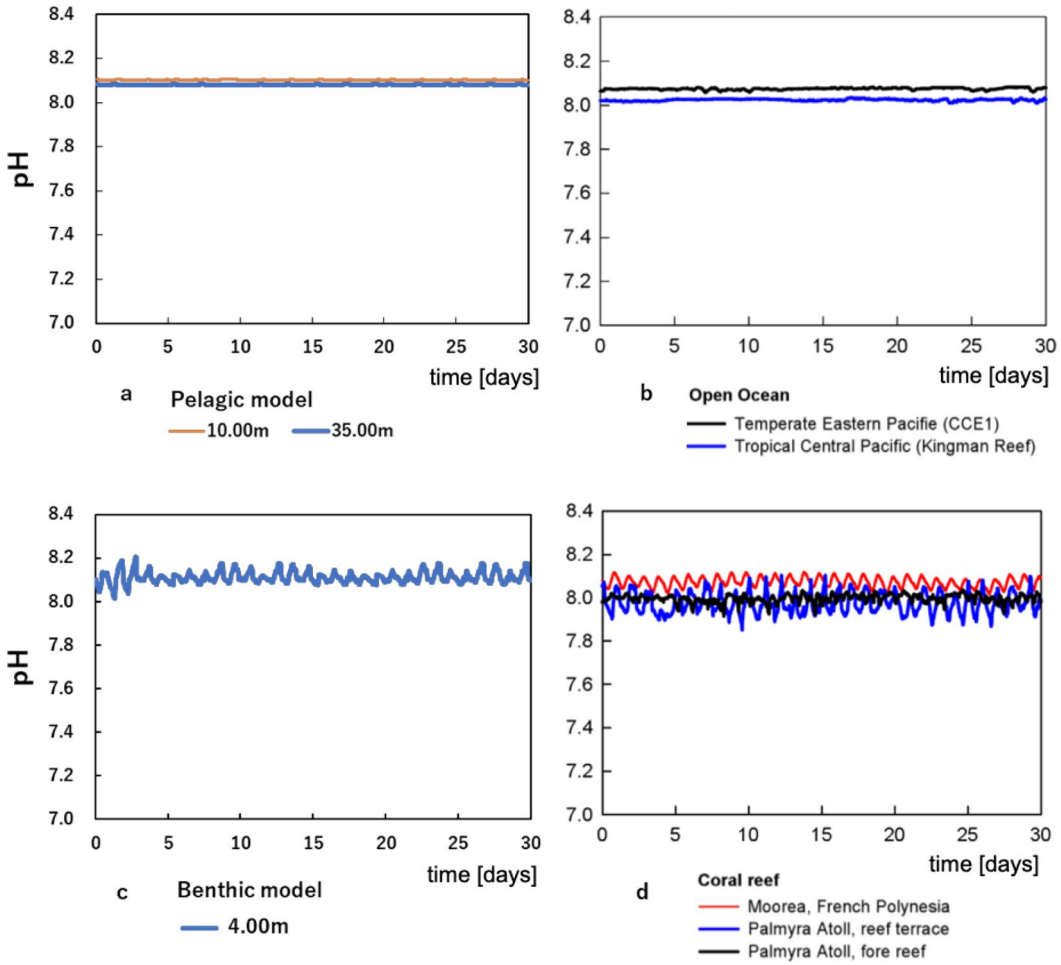

Fig. 6 Comparison of simulated pH and observations[19])

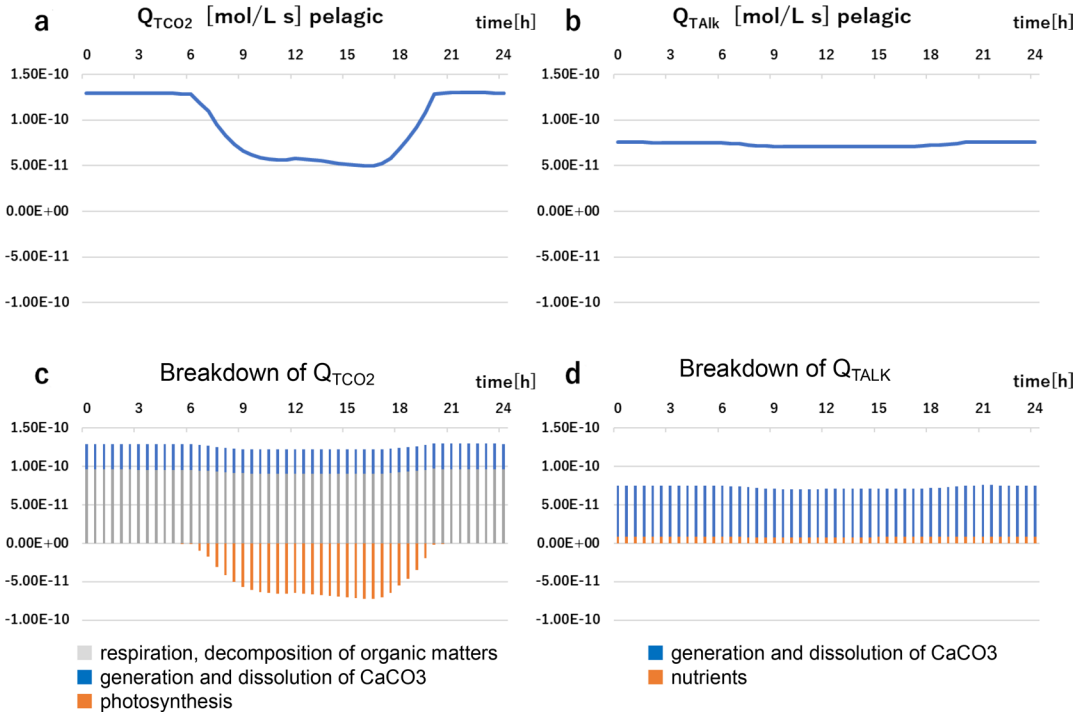

Fig. 7 Diurnal changes in Q_{TCO2} and Q_{TAlk} (**a**, **b**) and their breakdown (**c**, **d**) calculated by the pelagic submodel

4 Application to OTEC plant

The developed model was applied to determine the environmental changes due to the discharged water from an OTEC plant. The simulations were conducted for 1 MW-class OTEC and 10 MW-class OTEC. The depth of intake of deep seawater is assumed to be 800 m for the 1 MW-class OTEC and 1000 m for the 10 MW-class OTEC. The surface and deep seawater were mixed in the plant and discharged on the coastline (the depth of 0 m). The water qualities of the discharged water other than pH were calculated by taking the volume-weighted average of the surface and the deep seawaters, and pH was calculated by the chemical equilibrium. The water qualities of the surface water, deep seawater, and discharged water are shown in Table 3.

The changes in temperature, NO_3, and, pH in the bottom layer caused by the discharged water from the OTEC plant are shown in Fig. 8. The result are after 10-days discharge when they reached an almost steady state.

For the 1 MW-class OTEC, the water temperature declined by about 1.0 °C near the discharge location. The affected area spread in the shallow area along the coastline. However, the plant influence decreased rapidly as the water depth increased because the original temperature decreased. The concentration of NO_3 rose by about 5.0 µmol L^{-1} in the grid of the discharge location; however, the increase was less than 1.0 µmol L^{-1} in other areas. Negative impacts on coral could appear when the NO_3 concentration is higher than 1–5 µmol L^{-1} [43–45]. Therefore, the increase in NO_3 concentration would not have a serious impact on coral (Fig. 9).

Table 3 Water qualities of water discharged from the OTEC plant

	Surface water (10 m)	Deep seawater		Discharged water	
		(800 m)	(1000 m)	(1 MW)	(10 MW)
Flow rate [m^3 s^{-1}]	3.6 43	2.8 –	– 40	6.4	83
Temperature [℃]	28.8	5.4	4.4	18.5	17.0
NO_3 [µmol L^{-1}]	0.14	7.9	8.4	3.5	4.1
TCO2 [µmol L^{-1}]	1915	2265	2290	2068	2096
Talk [µmol L^{-1}]	2250	2360	2375	2298	2310
pH	8.11	7.60	7.57	7.90	7.88

The pH decreased by about 0.1 units in the grid of the discharge location, but the change was smaller in other areas. Impacts on coral are expected to appear at pH values around 7.7–7.9 [6, 7, 46]; therefore, the simulated pH will not affect the coral habitat. The results of the simulation confirmed that the impact of water discharged from a 1 MW OTEC plant will change the water quality to some extent, but the impacts on coral will be limited to the vicinity of the discharge point.

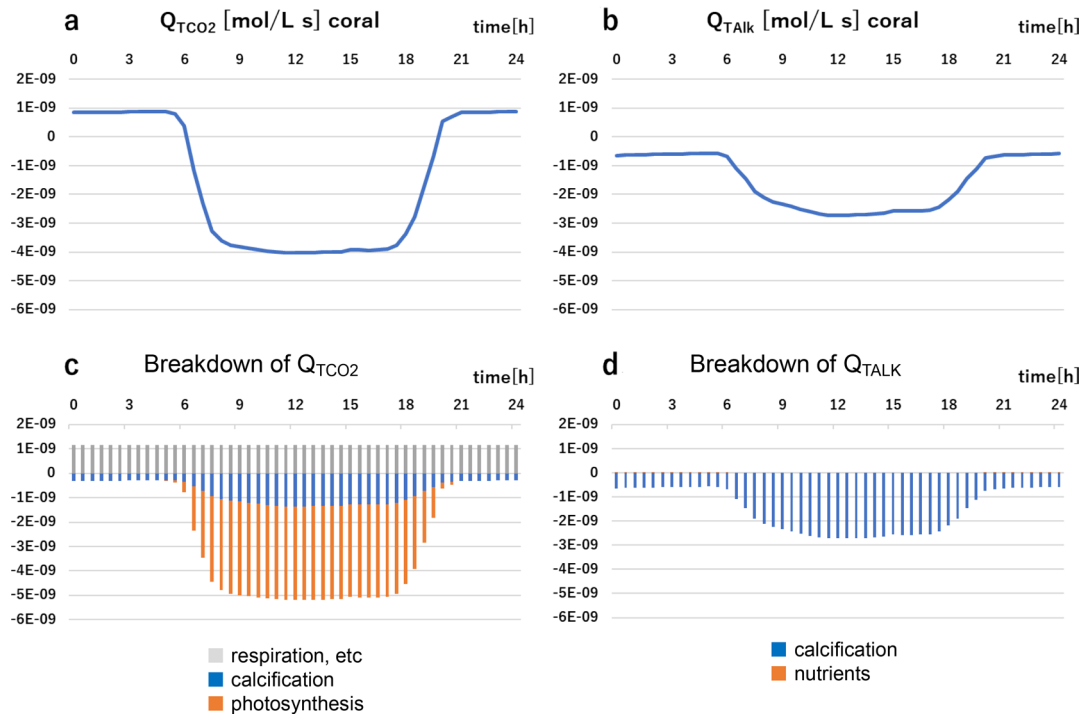

Fig. 8 Diurnal changes in Q_{TCO2} by coral and Q_{TAlk} (**a**, **b**) and their breakdown (**c**, **d**)

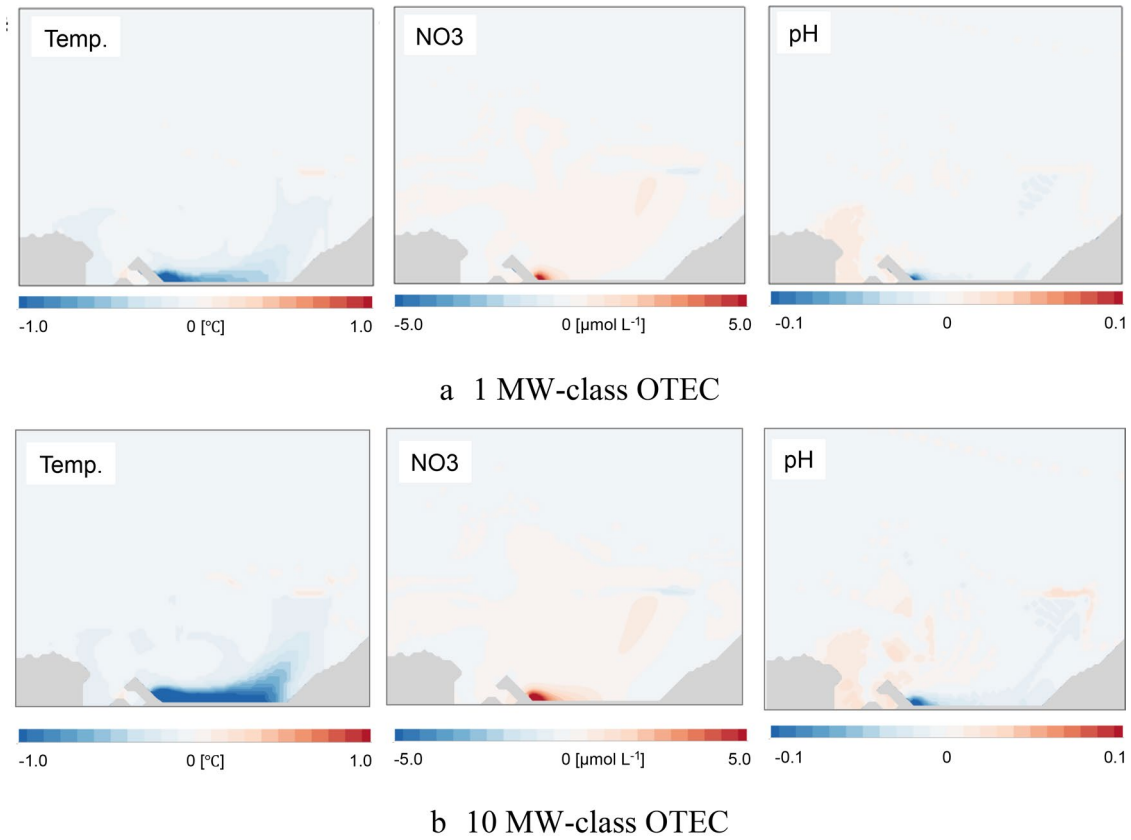

Fig. 9 Changes in the distribution of temperature, NO_3, and pH on the seafloor due to operation of OTEC plant

For the 10 MW-class OTEC, the wider area was affected by the discharged water. Especially in the vicinity of the discharge location, negative impacts on coral could appear due to the rise of NO_3 concentration. The decrease of pH was still within the range of no adverse impacts on coral.

5 Conclusions

We developed an ecosystem model for a subtropical shallow-water region that combines a pelagic submodel, a chemical equilibrium submodel, and a benthic submodel, and we successfully reproduced the diurnal changes in water quality, including pH changes. This model can consider both coral and phytoplankton impacts at the same time, and it is suitable for assessing the environmental impact of water discharged from an OTEC plant.

The developed model was used to predict the environmental impact of the water discharged from the OTEC plant. The simulation results suggest that a 1 MW-class OTEC plant would cause few environmental changes that would affect corals. For the 10 MW-class OTEC, negative impacts on coral could appear due to the rise of NO_3 concentration in the vicinity of the discharge location.

In this study, a framework of the model including pH changes due to both pelagic and benthic ecosystems were proposed and established, which will be useful to assess the impacts of OTEC. The basic performance of the model was confirmed such as diurnal variations of water qualities, influences of discharge waters from the OTEC plant. However, the validation of the model should be further conducted by using conditions of the specific site. Simulations for various conditions will also be necessary to discuss the environmental impacts due to OTEC comprehensively.

Acknowledgements This research was partially supported by JSPS KAKENHI (Grant 15H04210).

References

1. Kondo J ed (2015)Utilization technology for marine Energy - Power generation mechanisms and examples, Morikita Publishing Co., Ltd, 176pp (in Japanese).
2. Fujita RA, Markham J, Diaz Diaz J, Garcia JRM, Greenfield P, Black P, Aguilera S (2012) Revisiting ocean thermal energy conversion. Mar Policy 36:463–465
3. Kumejima-Town (2011) Basic research report on multiple utilization of Kumejima deep seawater, 190 pp (in Japanese)
4. Kleypas J, Feely R, Fabry V, Langdon C, Sabine C, Robbins L (2006) Impacts of ocean acidification on coral reefs and other marine calcifiers: a guide for future research. Report of workshop, sponsored by NSF, NOAA, and the U.S. Geological Survey
5. Anthony KR, Kline DI, Diaz-Pulido G, Dove S, Hoegh-Guldberg O (2008) Ocean acidification causes bleaching and productivity loss in coral reef builders. Proc Nat Acad Sci USA 105:17442–17446
6. Movilla J, Calvo E, Pelejero C, Coma R, Serrano E, Fernández-Vallejo P, Ribes M (2012) Calcification reduction and recovery in native and non-native Mediterranean corals in response to ocean acidification. J Exp Mar Biol Ecol 438:144–153
7. Wijgerde T, Silva C, Scherders V, Bleijswijk J, Osinga R (2014) Coral calcification under daily oxygen saturation and pH dynamics reveals the important role of oxygen. Biol Open 3:489–493
8. Grandelli PE, Rocheleau G, Hamrick J, Church M, Powell B (2012) Modeling the physical and biochemical influence of ocean thermal energy conversion plant discharges into their adjacent waters. United States. https://doi.org/10.2172/1055480
9. Wang Z, Tabeta S (2017) Numerical simulations of ecosystem change due to discharged water from ocean thermal energy conversion plant. OCEANS 2017-Aberdeen, 1–5.
10. Kinoshita T, Tabeta S, Fujino M (2003) Numerical simulation of artificial purification system by using hydrostatic and FULL-3D combined model. In: Proceedings of ASME 2003 22nd International Conference on Offshore Mechanics and Arctic Engineering, 1, 743–747
11. Mizumukai K, Sato T, Tabeta S, Kitazawa D (2008) Numerical studies on ecological effects of artificial mixing of surface and bottom waters in density stratification in semi-enclosed bay and open sea. Ecol Model 214:251–270
12. Kishi M, Ito S, Megrey B, Rose K, Werner F (2011) A review of the NEMURO and NEMURO.FISH models and their application to marine ecosystem investigations. J Oceanogr 67:3–16
13. Yamanaka Y, Yoshie N, Fujii M, Aita M, Kishi M (2004) An ecosystem model coupled with nitrogen-silicon-carbon cycles applied to Station A7 in the Northwestern Pacific. J Oceanogr 60:227–241
14. Lewis E, Wallace D (1998) Program Developed for CO2 System Calculations; Oak Ridge National Laboratory: Oak Ridge, TN. http://cdiac.ornl.gov/ftp/co2sys/
15. Feely RA, Sabine CL, Lee K, Berelson W, Kleypas J, Fabry VJ, Millero FJ (2004) Impact of anthropogenic CO_2 on the $CaCO_3$ system in the oceans. Science 305:362–366
16. Kuroyanagi A, Kawahata H, Suzuki A, Fujita K, Irie T (2009) Impacts of ocean acidification on large benthic foraminifers: results from laboratory experiments. Marine Micropaleontol 73:190–195
17. Dickson AG, Millero FJ (1987) A comparison of the equilibrium constants for the dissociation of carbonic acid in seawater media. Deep Sea Res Part A Oceanogr Res Pap 34(10):1733–1743
18. Uppstrom LR (1974) The boron/chlorinity ratio of deep-sea water from the Pacific Ocean. Deep Sea Res 21:161–162
19. Hofmann GE, Smith JE, Johnson KS et al (2011) High-frequency dynamics of ocean pH: a multi-ecosystem comparison. PLoS ONE 6:e28983
20. Santos I, Glud R, Maher D, Erler D, Eyre B (2011) Diel coral reef acidification driven by porewater advection in permeable carbonate sands, Heron Island. Great Barrier Reef Geophys Res Lett 38:L03604
21. Kleypas JA, Anthony KN, Gattuso J (2011) Coral reefs modify their seawater carbon chemistry–case study from a barrier reef (Moorea, French Polynesia). Glob Chang Biol 17:3667–3678
22. Anthony KN, Kleypas JA, Gattuso J (2011) Coral reefs modify their seawater carbon chemistry–implications for impacts of ocean acidification. Glob Chang Biol 17:3655–3666
23. Mongin M, Baird M (2014) The interacting effects of photosynthesis, calcification and water circulation on carbon chemistry variability on a coral reef flat: a modelling study. Ecol Model 284:19–34

24. Nakamura T, Nakamori T (2007) A geochemical model for coral reef formation. Coral Reefs 26:741–755
25. Atkinson MJ, Smith SV (1983) C: N: P ratios of benthic marine plants. Limnol Oceanogr 28:568–574
26. Darwin C (1842) The structure and distribution of coral reefs. Being the First Part of the Geology of the Voyage of the Beagle, under the Command of Capt. Fitzroy, R.N. during the Years 1832 to 1836. Smith Elder.
27. Mumby PJ, Steneck RS (2018) Paradigm lost: dynamic nutrients and missing detritus on coral reefs. Bioscience 68:7
28. Tanaka Y, Grottolib AG, Matsuib Y, Suzukic A, Sakai K (2015) Partitioning of nitrogen sources to algal endosymbionts of corals with long-term15N-labelling and a mixing model. Ecol Model 309:163–169
29. Tanaka Y, Suzuki A, Sakai K (2018) The stoichiometry of coral-dinoflagellate symbiosis: carbon and nitrogen cycles are balanced in the recycling and double translocation system. ISME J 12:860–868
30. de Goeij JM, van Oevelen D, Vermeij MJA, Osinga R, Middelburg JJ, de Goeij APFM, Admiraal W (2013) Surviving in a marine desert: the sponge-loop retains resources within coral reefs. Science 342:108–110
31. McMurray SE, Stubler AD, Erwin PM, Finelli CM, Pawlik JR (2018) A test of the sponge-loop hypothesis for emergent Caribbean reef sponges. Mar Ecol Prog Ser 588:1–14
32. Mueller B, den Haan J, Visser PM, Vermeij MJA, van Duyl FC (2016) Effect of light and nutrient availability on the release of dissolved organic carbon (DOC) by Caribbean turf algae. Sci Rep 6:18715
33. Rix L, de Goeij JM, Mueller CE, Struck U, Middelburg JJ, van Duyl FC, Al-Horani FA, Wild C, Naumann MS, van Oevelen D (2016) Coral mucus fuels the sponge loop in warm- and cold-water coral reef ecosystems. Sci Rep 6:18715
34. Xiong X, Matsuda Y, Hashioka T, Ono T, Yamanaka Y (2015) Effect of seasonal change in gas transfer coefficient on air–sea CO2 flux in the western North Pacific. J Oceanogr 71:685–701
35. Weiss RF (1974) Carbon dioxide in water and seawater: the solubility of a non-ideal gas. Mar Chem 2:203–215
36. Wanninkhof R (1992) Relationship between wind speed and gas exchange over the ocean revisited. Limnol Oceanogr 12:351–362
37. Fujii T (2017) CO2 dynamics of the atmosphere and surface seawater in coastal zone. J Jpn Assoc Hydrolog Sci 47(2):107–118
38. Pan Y, You L, Li Y, Fan W, Chen CA, Wang B, Chen Y (2018) Achieving highly efficient atmospheric CO_2 uptake by artificial upwelling. Sustainability 10:664. https://doi.org/10.3390/su10030664
39. HOT-DOGS (Hawaii Ocean Time-series Data Organization & Graphical System), http://hahana.soest.hawaii.edu/hot/hot-dogs/bdisplay.html
40. Oshimi R (2019) Environmental impact prediction of discharged water from OTEC plant. (Unpublished master's thesis), The University of Tokyo
41. Keir RS (1983) Variation in the carbonate reactivity of deep-sea sediments: determination from flux experiments. Deep Sea Res 30:279–296
42. Sulpisa O, Lixa C, Muccia A, Boudreaub BP (2017) Calcite dissolution kinetics at the sediment-water interface in natural seawater. Mar Chem 195:70–83
43. Bell PR, Elmetri I (1995) Ecological indicators of large-scale eutrophication in the Great Barrier Reef lagoon. Oceanogr Lit Rev 12(42):1145
44. Costa OS, Leao Z, Nimmo M, Attrill M (2000) Nutrification impacts on coral reefs from northern Bahia, Brazil. Hydrobiologia 440:307–315
45. Kleypas JA, McManus JW, Menez LAB (1999) Environmental limits to coral reef development: where do we draw the line? Am Zool 39:146–159
46. Fabricius KE, Langdon C, Uthicke S, Humphrey C, Noonan S, G. De'ath, R. Okazaki, M. Nancy, M. Glas, and J. Lough, (2011) Losers and winners in coral reefs acclimatized to elevated carbon dioxide concentrations. Nat Clim Change 1:165–169